AGU PUBLICATIONS

JGR

Journal of Geophysical Research: Oceans

RESEARCH ARTICLE

10.1002/2014JC010326

Key Points:
- Ageostrophic secondary circulation (ASC) impacts the chlorophyll filaments
- Late summer, ASC leads to the development of high chlorophyll filaments
- Earlier summer, chlorophyll filaments are 3–4 times weaker

Correspondence to:
I. Shulman,
igor.shulman@nrlssc.navy.mil

Citation:
Shulman, I., B. Penta, J. Richman, G. Jacobs, S. Anderson, and P. Sakalaukus (2015), Impact of submesoscale processes on dynamics of phytoplankton filaments, *J. Geophys. Res. Oceans*, *120*, 2050–2062, doi:10.1002/2014JC010326.

Received 21 JUL 2014
Accepted 4 FEB 2015
Accepted article online 12 FEB 2015
Published online 27 MAR 2015

Impact of submesoscale processes on dynamics of phytoplankton filaments

Igor Shulman[1], Bradley Penta[1], James Richman[1], Gregg Jacobs[1], Stephanie Anderson[1], and Peter Sakalaukus[1]

[1]Oceanography Division, Naval Research Laboratory, Stennis Space Center, Mississippi, USA

Abstract In Monterey Bay, CA, during northwesterly, upwelling favorable winds, the development of a southward flowing cold jet along the entrance to the Bay is often observed. This dense cold jet separates warm waters of the anticyclonic circulation offshore from the water masses inside the Bay. Interactions between the cold jet and the offshore anticyclonic circulation generate ageostrophic secondary circulation (ASC) cells due to submesoscale processes as, for example, flow interaction with the development of surface frontogenesis and nonlinear Ekman pumping. Based on observations and modeling studies, we evaluate the impact of these submesoscale processes on the formation of chlorophyll *a* filaments during late spring-earlier summer, and late summer time frames. We show that during the late summer time frame, ASC leads to the development of filaments with high values of chlorophyll *a* concentration along the edge of the cold jet–in contrast to the earlier summer time, when the ASC mixes phytoplankton much deeper to the area below of the euphotic depth, and chlorophyll *a* filaments are 3–4 times weaker.

1. Introduction

Recently, there has been an increase in observational and modeling studies focusing on the impact of submesoscale processes on biological dynamics in the ocean [see, e.g., *Levy et al*., 2012, review]. It has been found that submesoscale processes with scales of O(1–10 km) in the horizontal, O(100 m) vertical, and O(1 day) temporal domains impact phytoplankton growth and increase productivity in a variety of ways, as for example, by modulating the vertical supply of nutrients into the euphotic, lighted layer, or by changing the light exposure of phytoplankton by modulating the strength of vertical mixing [*Levy et al*., 2012; *McGillicuddy et al*., 2003; *Gruber et al*., 2011; *Capet et al*., 2008; *Mahadevan and Archer*, 2000; *Allen et al*., 2005; *Lapeyre and Klein*, 2006; *Nagai et al*., 2008; *Calil and Richards*, 2010; *Pallàs-Sanz et al*., 2010]. These processes contribute to the development of 5–10 km wide submesoscale filaments in the form of streaky chlorophyll patches often observed in satellite images of ocean color. As stated in *Levy et al*. [2012], the impact of submesoscale processes on the intensification of phytoplankton filaments depends on the local hydrography, euphotic depth, and nutrient distributions.

During upwelling favorable winds, pockets of cold, salty water appear to the north of Monterey Bay, CA. These pockets grow into a cold, dense jet extending offshore and flowing southward along the entrance to the Bay [*Rosenfeld et al*., 1994; *Ramp et al*., 2009]. The cold, dense jet interacts with the warmer, less saline anticyclonic circulation offshore [*Breaker and Broenkow*, 1994; *Rosenfeld et al*., 1994; *Paduan and Rosenfeld*, 1996; *Ramp et al*., 2009]. This feature is associated with the larger-scale, meandering California Current System and is not locally generated [*Brink et al*., 1991; *Breaker and Broenkow*, 1994; *Rosenfeld et al*., 1994]. The anticyclonic California Current meander, also some-times referred to as the Monterey Bay Eddy (MBE), is a frequently observed feature of the region during the upwelling [*Rosenfeld et al*., 1994; *Ramp et al*., 2005, 2009]. The MODIS-Aqua SSTs for 11, 13, and 15 August 2003 (Figure 1a) illustrate well the described dynamics during the upwelling event: the development and intensification of a southward flowing cold jet and its interaction with the warm offshore anticyclonic circulation. The MODIS-Aqua chlorophyll a images show streaky filaments (5–10 km wide) along the offshore edges of the jet (Figure 1). Figure 1 shows that filaments are connected to the high chlorophyll water masses to the north of the Bay, and because of a predominately southward flow during the upwelling, we can suspect that the advection of relatively high chlorophyll water masses from the north contributed to the development of the narrow filaments in

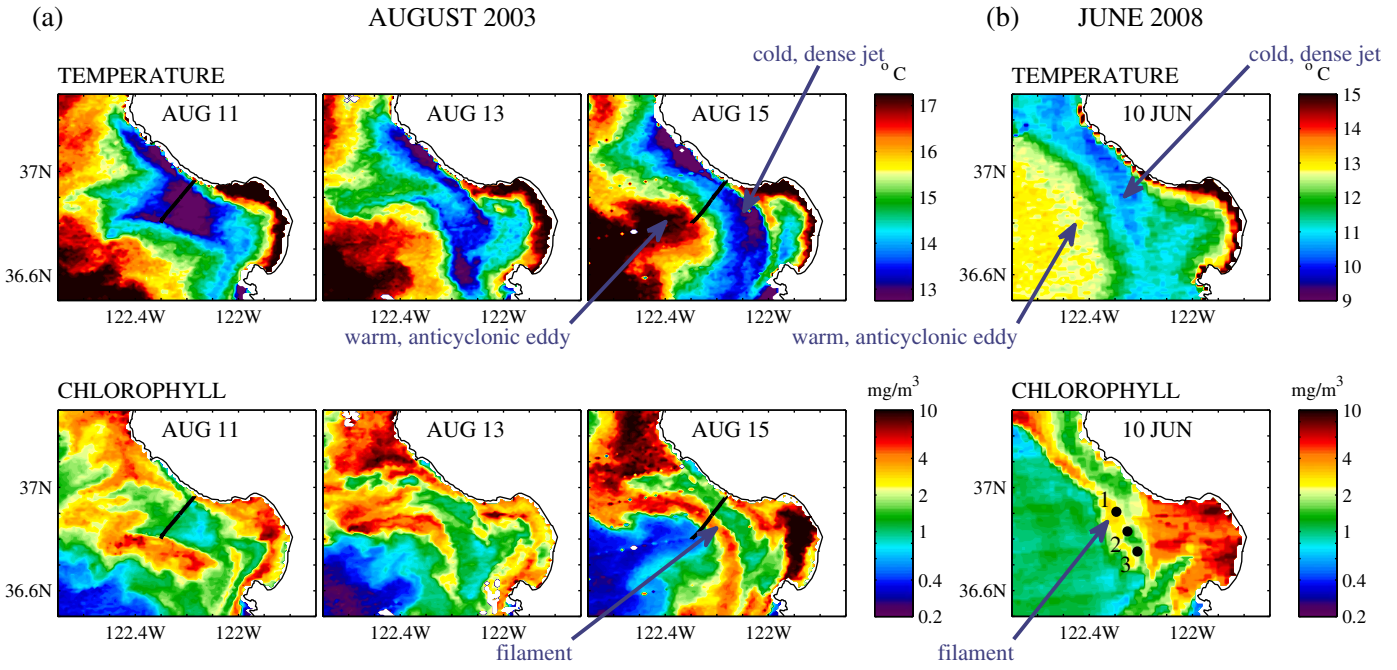

Figure 1. MODIS-Aqua SST and Chlorophyll *a* images for August 2003 (a) and June 2008 (b). Figure 1a Black lines on MODIS SST and Chlorophyll a images indicate AUV DORADO sections taken 11 and 16 August. Figure 1b Black dots on MODIS Chlorophyll *a* image for 10 June 2008 indicate locations of The R/V Point Sur stations.

Figure 1. At the same time, Figure 1 shows that these narrow filaments are maintained in the frontal area between the meandering warm anticyclonic circulation offshore and the cold jet. It is known[*Calil and Richards*, 2010; *Pallàs-Sanz et al.*, 2010; *Levy et al.*, 2012], that the area between a cold jet and warm anticyclonic circulation is prone to generation of submesoscale processes, which contribute to the development of narrow, streaky chlorophyll filaments like those presented in Figure 1.

It is challenging to reliably quantify the contributions of phytoplankton advection versus in situ processes to the development and intensification of submesoscale filaments. There is a lack of high-resolution surface and subsurface (Lagrangian and Eulerian-type) bio-optical and physical observations and the present maturity level of bio-optical models does not provide the needed capabilities, especially at submesoscale.

In the present paper, using available bio-optical, physical observations and a well-established physical model, we want to address the following questions: Are the observed streaky chlorophyll a offshore filaments (Figure 1) in the Monterey Bay area locally intensified by the submesoscale processes? Observations of ocean color show different intensities of observed submesoscale filaments (for example, the intensity of the August 2003 filament is 3–4 times higher than the June 2008 filament, Figure 1). What are the reasons for the observed differences in chlorophyll a concentrations of the August 2003 and June 2008 filaments (Figure 1)?.

To answer these questions, we have organized the paper as follows: Section 2 describes observations and models used in this study. Results are presented in section 3. Section 4 is devoted to discussions and conclusions.

2. Methods

2.1. Observations

2.1.1. Satellite MODIS-Aqua Ocean Color Data

The MODIS-Aqua satellite imagery was processed using the NRL Automated Processing System (APS). APS is a complete end-to-end system that includes sensor calibration, atmospheric correction (with near-infrared correction for coastal waters), and bio-optical inversion. APS incorporates, and is consistent with,

the latest NASA MODIS code (SeaDAS) [*Gould et al*., 2011; *Martinolich and Scardino*, 2011]. In this study, estimates of the chlorophyll *a* (Chl) from MODIS-Aqua imagery for 11–15 August of 2003 and 10 June of 2008 were used. Chlorophyll data are derived by OC3M algorithm [*O'Reilly et al*., 2000] at 1 km pixel resolution. The diffuse attenuation coefficient Kd (488) was estimated in accord with *Lee et al*. [2005]. The Kd (488) was used to estimate the euphotic depth (noted Eu); the Eu was estimated as the depth where photosynthetic available radiation (PAR) is 1% of its surface value [*Lee et al*., 2007]:

$$Eu = -\ln(0.01)/Kd(488)$$

2.1.2. Mooring Data

Observations of winds and PAR from the Monterey Bay Aquarium Research Institute (MBARI) surface moorings M1 (122.02° W, 36.74° N) and M2 (122.40° W, 36.67° N) are used in this study (Figure 2). Near-surface 3m wind speed and direction were measured by a MetSys monitor. The observed PAR was measured by the spectroradiometer mounted on moorings approximately 3 m above the water surface [*Chavez et al*., 2000].

2.1.3. HF Radar Surface Currents

Surface current observations used in this study were derived from the California Coastal Ocean Current Mapping Program's HF radar network (www.cocmp.org). Surface currents were estimated based on inputs from five HF radar sites for August 2003 and seven HF radar sites for June 2008. Vector currents were estimated on a Cartesian grid with a horizontal resolution of 3 km by computing the best-fit vector velocity components using all radial velocity observations within a radius of 3 km for each grid point each hour [*Paduan et al*., 2006].

2.1.4. Water Samples

The R/V Point Sur occupied hydrographic and optical stations from 2 to 13 June 2008. Temperature and salinity depth profiles binned to 1 m vertical resolution were derived from Sea-Bird SBE 9+ CTD measurements using standard Sea-Bird processing software. Nutrients analyses were performed on water samples from the Niskin bottle rosette in accord with *Pennington and Chavez* [2000]. Water samples (540 mL) collected from near-surface (~0.5m) Niskin bottles were filtered onto Whatman glass fiber filters (GF/F). High performance liquid chromatography (HPLC) analysis provided pigment indices and proportion factor for microplankton, nanoplankton, and picoplankton [*Vidussi et al*., 2001]. The pigment data indicated that the microplankton fraction was predominantly composed of diatoms (based on the presence of fucoxanthin).

2.1.5. Autonomous Underwater Vehicles (AUVs)

Propeller-driven AUV such as the MBARI manufactured DORADO have been described in *Bellingham et al*. [2000] and *Ryan et al*. [2009]. Deployments of the DORADO during 11 and 16 August 2003 are used in this study. The instruments on board included CTD, optical backscattering, chlorophyll fluorescence, nitrate, and bioluminescence potential sensors.

2.2. Model

The Monterey Bay circulation model used in this study has been described in detail elsewhere [*Shulman et al*., 2010, 2011]. The model domain is shown on Figure 2a. The model is based on the Navy Coastal Ocean Model (NCOM), which is a primitive-equation, 3-D, hydrostatic model. It uses the Mellor-Yamada level 2.5 turbulence closure scheme, and the Smagorinsky formulation for horizontal mixing. The Monterey Bay model uses the Navy Coupled Ocean Data Assimilation (NCODA) system [*Shulman et al*., 2011]. The NCODA assimilates satellite altimeter observations, satellite sea surface temperature, as well as available in situ vertical temperature and salinity profiles from ships and gliders. The Monterey Bay model predictions during August of 2003 and June 2008 were validated against assimilated observations (to verify that assimilation decreases misfits between the model and assimilated observations), as well as against nonassimilated observations: temperature, salinity, and currents profiles at moorings, HF radar-derived currents, and aircraft SSTs [*Shulman et al*., 2009, 2010, 2011, 2013]. The Monterey Bay model is forced with surface fluxes from the Coupled Ocean and Atmospheric Mesoscale Prediction System (COAMPS) [*Doyle et al*., 2009] at 3 km horizontal resolution. Comparisons of COAMPS predictions with observations from moorings and aircraft surveys were reported in *Ramp et al*. [2009], *Doyle et al*. [2009], *Chao et al*. [2009], and *Shulman et al*. [2009, 2010]. Comparisons demonstrated high complex correlations between the observed and COAMPS-

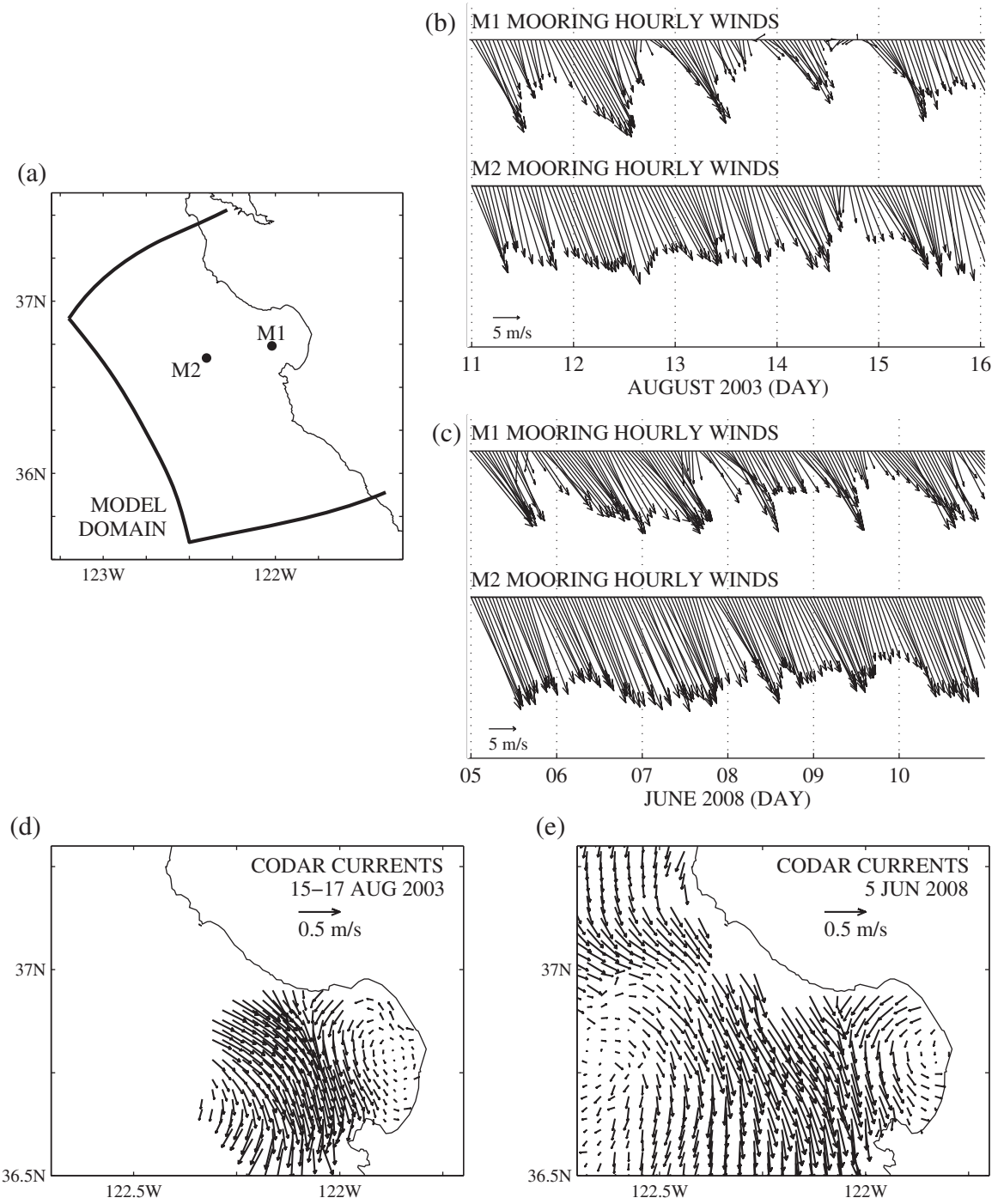

Figure 2. (a) Model domain with locations of moorings M1 and M2. (b) Observed wind velocities at moorings during 11–16 August 2003 and (c) 5–10 June 2008. (d) Observed HF Radar surface currents averaged over15–17 August 2003 (d), and for 5 June 2008 (e).

predicted wind velocities, and good agreement in magnitudes and the extent of each observed upwelling event. Comparisons of observed and COAMPS-predicted short-wave radiations (SWR) demonstrated the overestimation of the SWR in the COAMPS predictions at mooring locations, and for this reason COAMPS SWR values were adjusted to match observed mean daily values of SWR.

In this study, a depth of mixed layer (MLD) is derived from the Monterey Bay model and observations. In both cases, the MLD is computed as the depth at which temperature deviates by 0.3°C from the near-surface (at 2 m depth) temperature.

3. Results

The development and intensification of a southward flowing cold jet and its interaction with the warm offshore anticyclonic circulation are well illustrated by MODIS-Aqua SSTs for August 2003 on Figure 1a and by HF Radar surface currents averaged over 15–17 August 2003 on Figure 2d. At the edges between the cold jet and warm anticyclonic circulation, there is a development of a narrow, submesoscale (~5–10 km wide) filament with high chlorophyll *a* concentration (Figure 1a).

Because the location of the submesoscale filament (Figure 1a) coincides with the area between the cold jet and the anticyclonic circulation offshore, the submesoscale process due to their flow interaction with the development of the surface frontogenesis is considered here [*Hoskin*, 1982; *Levy et al*., 2012; *Calil and Richards*, 2010]. Because the upwelling favorable winds have been blowing along the jet and over the anticyclonic circulation for more than a week (Figure 2b), the second submesoscale process considered here is due to the forcing interaction—nonlinear Ekman transport [*Thomas and Lee*, 2005; *Levy et al*., 2012; *Calil and Richards*, 2010]. Both submesoscale processes are likely to contribute to the development and intensification of the submesoscale filament [*Calil and Richards*, 2010].

In the first process, the interaction between the dense cold jet and lighter, warmer, anticyclonic circulation leads to an ageostrophic secondary circulation (ASC). These ASC cells are generated in a plane perpendicular to the density front [*Hoskins*, 1982], which are upward (upwelling) on the light (anticyclonic) side of the front and downward on the dense side of the front. The ASC cells lead to a restratification flow from the light site to the dense. In *Hoskin* [1982], the vector Q_1 is used to qualitatively diagnose ageostrophic vertical motion due to frontogenesis:

$$Q_1 = \left(-\frac{\partial u_g}{\partial x}\frac{\partial b}{\partial x} - \frac{\partial v_g}{\partial x}\frac{\partial b}{\partial y}, -\frac{\partial u_g}{\partial y}\frac{\partial b}{\partial x} - \frac{\partial v_g}{\partial y}\frac{\partial b}{\partial y} \right) \tag{1}$$

where u_g and v_g are the horizontal geostrophic velocities, and $\frac{\partial b}{\partial x}$ and $\frac{\partial b}{\partial y}$ are the horizontal gradients of buoyancy:

$$b = -g\frac{\rho^*}{\rho_0} \tag{2}$$

with ρ^* being the deviation from the reference density ρ_0, and g is the acceleration due to gravity. The local maximum of Q_1 creates a vertical circulation with associated upwelling/downwelling ACS cells. Vertical velocity due to frontogenesis (noted here by W_{af}) is estimated from the vorticity equation [*Hoskin*, 1982] with boundary condition at surface $W_{af} = 0$.

The second process is the intensification of ASC cells due to nonlinear Ekman transport [*Thomas and Lee*, 2005; *Levy et al*., 2012]. This is a result of downfront winds blowing in the direction of the frontal jet. When a wind blows down a front, cross-front advection of density by Ekman flow results in a destabilization of the water column, which results in a convection that is localized to the front. The vertical circulation associated with the ASCs is characterized by subduction on the dense side of the front and upwelling along the frontal interface. It creates upwelling on the anticyclonic circulation site (with negative relative vorticity) and downwelling on the jet site. According to *Thomas and Lee* [2005], the dominant term in nonlinear Ekman transport is:

$$Me = -\frac{\tau_a}{\rho_0(f+\xi)} \tag{3}$$

where *Me* is nonlinear Ekman transport, τ_a is along-front wind stress component, f is Coriolis parameter, and ξ is relative vorticity of geostrophic flow, and the leading order term of the nonlinear Ekman pumping (NLEP) is:

$$W_{nlep} = \frac{1}{\rho_0}\mathbf{z}\cdot\nabla\times\frac{\tau}{(f+\xi)} \tag{4}$$

where, τ is surface wind stress.

Our objective is to demonstrate whether surface frontogenesis (represented by Q1 (1)) and nonlinear Ekman transport (represented by Me (3)) contributed to the development of chlorophyll a filament

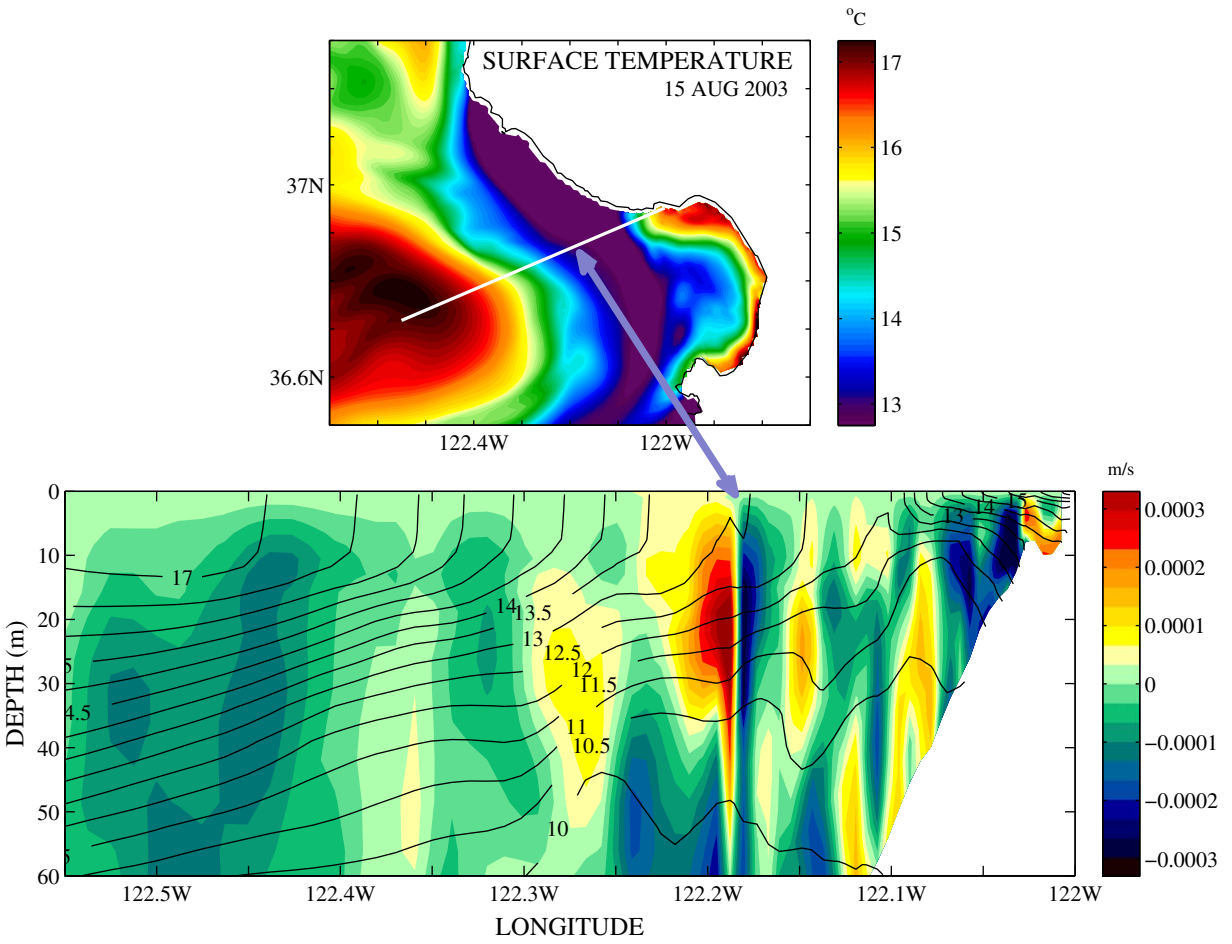

Figure 3. (top) the model SST (15 August 2003) with the location of cross section; (bottom) the model vertical velocity with the model potential temperature isotherms.

(Figure 1a). The local maxima of Q_1 and *Me* create a vertical circulation with associated upwelling/downwelling ACS cells. For both processes, ASC cells are upward (upwelling) on the light (anticyclonic) side of the front, and downward on the dense side of the front. The ASC cells modulate the mixing of material down to the mixed layer depth (MLD), provide injections and cycling of nutrients, as well as the cycling of phytoplankton in the subsurface down to the base of the mixed layer depth. All these directly influence the intensification and development of submesoscale phytoplankton filaments.

Figure 3 shows the model vertical velocity and the potential temperature for a section across the cold filament, the warm offshore anticyclonic circulation, and the frontal area between them.

The model vertical velocity and subsurface temperature show the development of the ACS cell, with the ascending part of this cell coinciding with the warm part of the front. This is in agreement with what would be expected from the surface frontogenesis and nonlinear Ekman transport.

Figures 4a and 5 show observed and modeled-predicted properties plotted along the section crossing the submesoscale filament. On Figure 4a, the vector *Q*1 magnitude (1), the value of nonlinear Ekman transport *Me* (3) and the NLEP (W_{nlep}) were estimated by using the COAMPS wind stress and the Monterey Bay model fields of temperature, salinity, and velocity averaged over a period of 48 h centered on 15 August 00Z 2003. Estimated values of Q1, Me, and W_{nlep} were averaged over the top 15 m depth (Figure 4a, third row), which is the depth of model-predicted MLD (Figure 4a, second row). On Figure 5, the model vertical velocity (W), the W_{nlep}, and the vertical velocity due to frontogenesis (W_{af}) are plotted along the same section as on Figure 4a. All three velocities were averaged over a period of 48 h centered on 15 August 00Z and over the top 15 m depth. Locations of the local maximum of Q1 (1) and *Me* (3) coincide with the location of the filament.

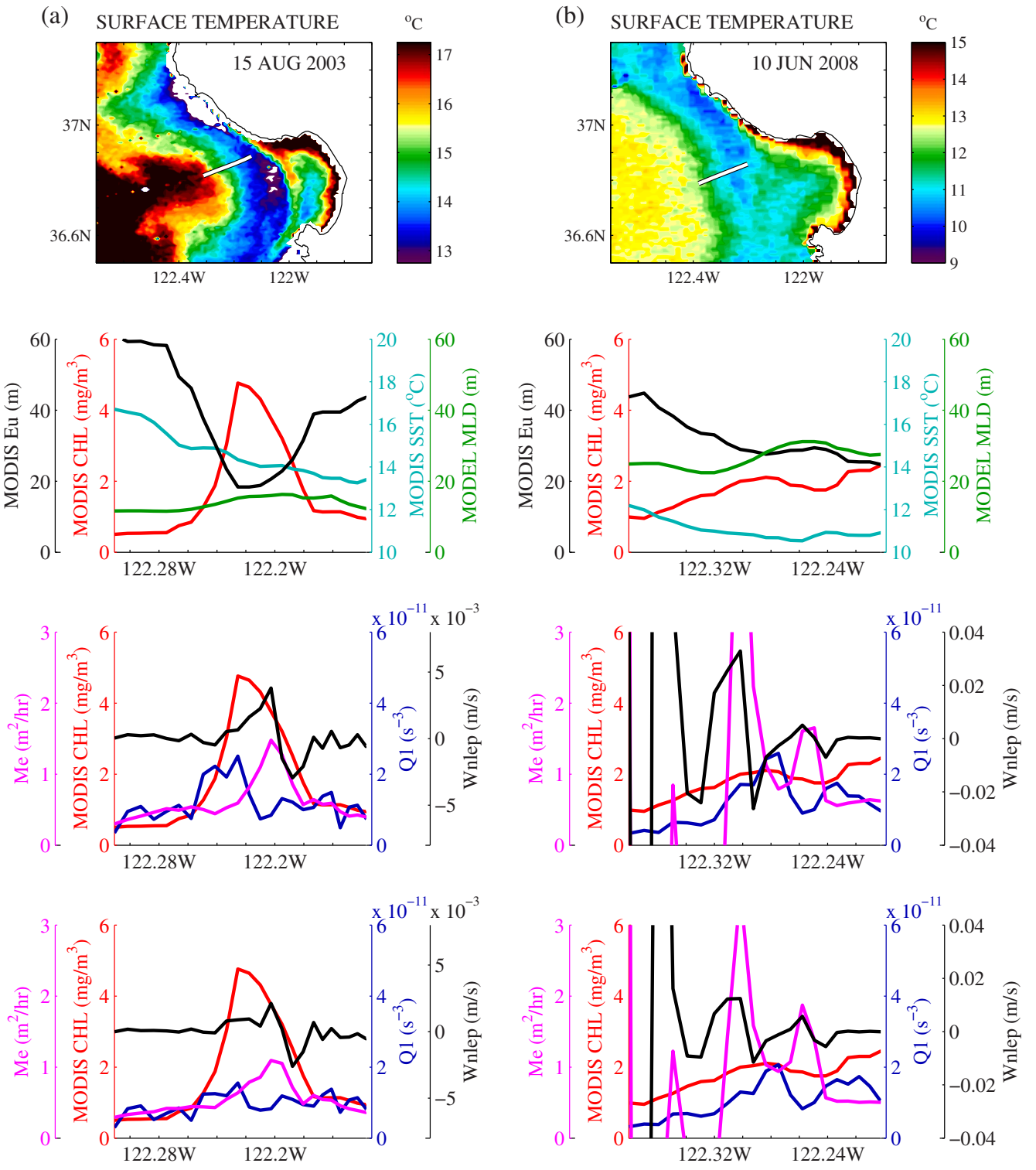

Figure 4. Observed and model predicted properties plotted along sections crossing filaments on (a) 15 00Z August 2003 and (b) 10 00Z June 2008. Sections are indicated by white lines on MODIS-Aqua SST images (top row). Plots along the section of: (second row) MODIS-Agua chlorophyll *a* (red) and SST (light blue), euphotic depth Eu (black) derived from the MODIS-Aqua observations, and the mixed layer depth MLD (green) derived from the model; (third row) MODIS-Agua chlorophyll *a* (red), magnitudes of vector Q1 (blue), nonlinear Ekman transport *Me* (magenta), and nonlinear Ekman pumping W_{nlep} (black), which are averaged over top 15m depth; (bottom row) MODIS-Agua chlorophyll *a*, magnitudes of vector Q1, nonlinear Ekman transport Me and nonlinear Ekman pumping W_{nlep}, which are averaged over top 40 m depth. Note, that scales of W_{nlep} for 2003 and 2008 are different.

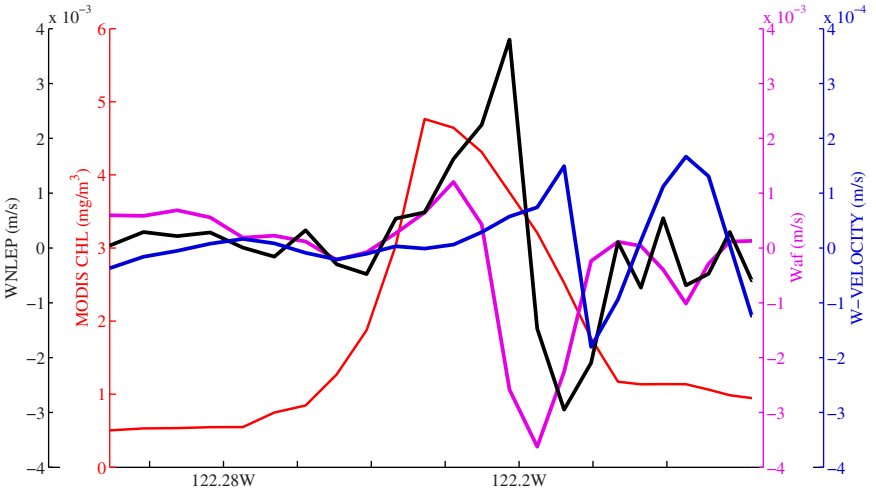

Figure 5. The model vertical velocity W (blue), the nonlinear Ekman pumping W_{nlep} (black), and the vertical velocity due to frontogenesis W_{af} (magenta) are plotted along the same section as on Figure 4a. All three velocities are averaged over a period of 48 h centered on 15 August 00Z and over the top 15 m depth.

In the area of the chlorophyll a filament, all three vertical velocities show upwelling on the warm side of the front and downwelling on the cold jet side, which is in agreement with the development of ACS cells due to the nonlinear Ekman transport and the surface frontogenesis. The same order of W_{nlep} and W_{af} indicate that both submesoscale processes (the nonlinear Ekman pumping and the surface frontogenesis) are important processes in the upper ocean dynamics during the formation and development of the filament. With the MLD around 15 m and vertical velocities of order 10^{-4}–10^{-3}, the time scales of considered submesoscale processes are around 0.17–1.7 days. These time scales are in the ranges of observed time scales of phytoplankton growth rates [*Landry et al*., 2009; *Waterhouse and Welschmeyer*, 1995]. With spatial scales of 10–50 km, the time scale for horizontal advection by typical surface velocities of order 0.2–0.4 m/s (Figure 2d) is around 0.3–3 days. Therefore, considered submesoscale processes, horizontal advection, and phytoplankton growth rates had similar time scales during the development of the observed chlorophyll a filament. Note, that the vertically averaged model vertical velocity (W) is about an order smaller than vertically averaged W_{nlep} and W_{af}. *Calil and Richards* [2010] also reported larger values of vertically averaged W_{nlep} in comparison to the vertically averaged model vertical velocity.

Figure 6 presents subsurface properties along the AUV DORADO surveys. On 16 August, the figure shows the deepening of isotherms offshore at the end of the section where the section reaches the warm, anticyclonic circulation offshore (see position of the section over 15 August MODIS SSTs on Figure 1 of the paper, top). Also, there is a flattening of isotherms as the section moves from the warm anticyclonic circulation through the frontal area. This is consistent with the surface frontogenesis, which tends to flatten the isopycnals/isotherms [see, e.g., *Klein and Lapeyre*, 2009]. In the area of filament, both model-predicted MLD (∼15 m, Figure 4a, second row) and observed MLD (∼15 m, Figure 6, 16 August) are shallower then the estimated euphotic depth (Eu) in and around the filament (Figure 4a, second row). In this case, the developed ASC cells kept phytoplankton in the lighted area and supported photosynthesis. Also, the ASC cells provided a vertical supply of nutrients into the euphotic area and facilitated consumption of nutrients (see uplifting of nutricline in the area of the filament on 16 August, Figure 6).

In the area of the filament, the observed changes in subsurface properties show the shallowing of MLD, increase in consumption of nutrients, and increase in subsurface values of chlorophyll, optical backscattering and bioluminescence potential from 11 to 16 August (Figure 6). DORADO surveys (16 August) show a coincidence of high values in observed chlorophyll a, BL potential, and optical backscattering in the area of the filament. *Moline et al*. [2009] demonstrated that such a coincidence of high values in considered bio-optical parameters is associated with the presence of bioluminescent species of dinoflagellates in the northern part of the Monterey Bay. Based on this, we suspect that the observed coincidence of high values of chlorophyll a, BL potential, and optical backscattering point to a presence of the bioluminescent dinoflagellates in the offshore submesoscale filament.

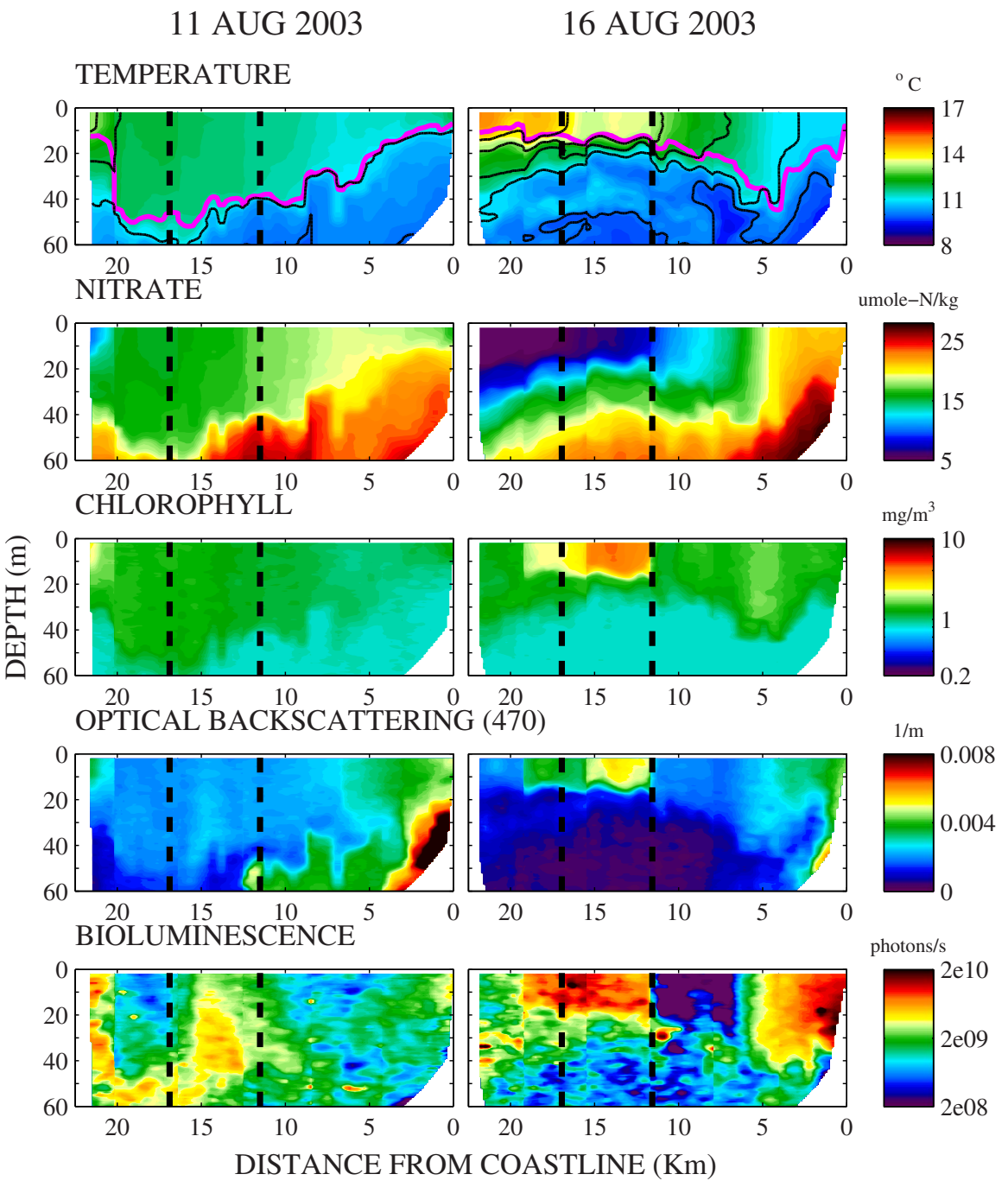

Figure 6. AUV DORADO surveys taken 11and 16 August 2003. Isotherms are shown in black, and estimated mixed layer depths (MLD) are shown in magenta on temperature plots (top). Vertical-dashed lines indicate location of the high chlorophyll *a* filament: 11 August—where the filament appeared later on MODIS-Aqua image on 15 August; 16 August—where the filament observed in MODIS-Aqua image on 15 August.

Figure 1 provides comparisons of the MODIS-Aqua chlorophyll *a* and SST images for August 2003 and June 2008. As for August 2003, images for 10 June of 2008 also show a development of a chlorophyll *a* submesoscale filament in the area between the cold dense upwelling jet and the warm anticyclonic circulation. The horizontal cross-shore scales of both (August 2003 and June 2008) filaments are very similar (5–10km). However, the maximum of the June filament chlorophyll *a* is about 3–4 times smaller than in August 2003 (Figure 1). Figure 1 and 2 indicate that hydrographic conditions were very similar during both time periods (August 2003 and June 2008): (1) steady upwelling favorable winds with comparable magnitudes; (2) development of

cold, southward flowing jet along the entrance to the Bay, and (3) the presence of warm anticyclonic circulation offshore. Both filaments, August 2003 and June 2008 (Figure 1), coincide with areas between the cold, dense jet and the warmer, anticyclonic circulation offshore. This indicates that ageostrophic secondary circulation cells due to submesoscale processes (surface frontogenesis and nonlinear Ekman transport) also impacted the development and intensity of the June filament. The question is why the chlorophyll *a* concentration of the June 2008 filament is 3–4 times lower than one in August 2003 (Figure 1)?.

One obvious reason is the temperature difference between August 2003 and June 2008 along the two patches. Figure 4b provides plots of observed and model-derived properties for 10 June of 2008 (which are also plotted for 15 August 2003 on Figure 4a). The difference between observed in August and June MODIS-Aqua SSTs is ~3°C (Figures 4a and 4b). The impact of temperature on the filaments growth can be estimated, for example, by using the relation between the maximum of phytoplankton growth and the temperature T [*Eppley*, 1972]:

$$\mu_{\max}(T) = \mu_0 * 1.066^T \quad (5)$$

where $\mu_{\max}$ is the maximum growth rate. According to (5), 3°C difference will result in a ~21% increase in the maximum phytoplankton growth rate. This alone does not explain the observed 3–4 times difference in intensity of phytoplankton filaments.

Table 1 presents observed nutrients (nitrate and silicate) at three stations taken on 10 June 2008 along the weak chlorophyll *a* filament (Figure 1b). According to Table 1, nitrate availability on June 10 2008 in the subsurface (down to 40 m depth) is much higher along the 10 June of 2008 filament than along the AUV DORADO survey on 16 August 2003 (Figure 6), indicating higher consumption of nitrate in August of 2003 than in June of 2008. HPLC samples analysis (section 2) demonstrated that microplankton (composed predominantly of diatoms) was about 80–85% of total phytoplankton population (diatoms plus nanoplankton and picoplankton) in the top 0.5 m at three stations on 10 June of 2008. Therefore, the filament of 10 June 2008 was mostly composed of diatoms (at least close to surface), which require silicate(Si(OH)4) for growth. According to Table 1, the ratio of $Si(OH)4/NO_3$ is around 1:1 or higher for all stations and depths, indicating ample silica was available in the water column for diatom growth [*Brzezinski*,1985]. Also, ratios of $Si(OH)4/NO_3$ at stations (Table 1) taken along the filament are comparable or even higher than observed ratios at stations (not shown here) taken in the more productive northern part of the Bay (Figure 1b). All the above indicate that conditions were not nutrient limited for the filament intensification and development in June 2008.

Observed daily averaged PAR values at mooring M1 were around 140 W/m^2 during 11–16 August 2003, and during 5–10 June 2008. At mooring M2, the observed daily averaged PAR values were higher (~150 W/m^2) during 5–10 June 2008 than during 11–15 August 2003 (~130W/m^2). Therefore, the available surface light for photosynthesis was comparable for both time periods. Estimates of euphotic depths (Eu) are ~20–30 m for 15 August 2003 (Figure 4a, second row) and ~30 m for 10 June 2008 (Figure 4b, second row) in the areas of two filaments. Therefore, based on the observed PAR and estimated euphotic depths, conditions of light availability in surface and subsurface were comparable for both of the considered time periods.

The mixed layer depth (MLD) for 10 June 2008 was estimated using the same criteria as for 15 August 2003 (Section 2). Based on temperature presented in Table1, the MLD is around 40 m for station 1 and between 40 and 60 m for stations 2 and 3. Therefore, MLD for 10 June 2008 is about 2–3 times deeper than MLD

Table 1. Observed Temperature, Nitrate, and Silicate at The R/V Point Sur Stations Taken on 10 June 2008

	T (°C)			NO_3 (μ mole/kg)			SiO_4 (μ mole/kg)		
	Stations			Stations			Stations		
Depth	1	2	3	1	2	3	1	2	3
0	9.98	9.6	9.96	21.3	23.0	21.4	26.3	22.9	20.7
5	9.97	9.59	9.93	23.9	24.3	21.8	27.9	24.5	21.1
10	9.97	9.58	9.93	23.5	24.6	21.6	27.2	24.9	21.1
20	9.92	9.58	9.91	23.7	24.9	21.3	28.6	25.0	21.0
30	9.86	9.5	9.86	23.5	22.9	21.9	28.6	22.1	21.7
40	9.66	9.35	9.69	24.6	27.2	22.7	28.8	28.8	23.1
60	9.41	9.03	9.64	25.0	29.1	23.4	32.8	33.8	26.4

observed during August 2003 (~15 m), and deeper about 10–20m than the estimated euphotic depth Eu (Figure 4b). Bear in mind that the Eu for August 2003 is deeper than observed MLD. Therefore, the discussed above ACS cells in June of 2008 (due to surface frontogenesis and nonlinear Ekman transport) transported phytoplankton out of the euphotic zone, reduced the presence of phytoplankton in the lighted area, and reduced the exposure of phytoplankton to light, and, therefore limited growth of the filament in June 2008. The *Q*1 magnitude (1), *Me* (3), and W_{nlep} (4) were estimated by the same procedure as for 15 00Z August 2003. Values of the Q1 magnitude, *Me*, and W_{nlep} (averaged over 40m (the observed MLD for June 2008)) are larger for 10 June 2008 (Figure 4b, bottom row) than corresponding values for 15 August 2003 (Figure 4a, bottom row). Note, that the MLD derived from the model predictions for 10 June of 2008 (Figure 4b, second row) is somewhat shallower than the observed MLD during this period (based on observed temperature, Table 1); therefore, we should expect that actual values of Q1, Me, and W_{nlep} are even larger than the model predicted for 10 June 2008, and certainly larger than the values for 15 August 2003. Therefore, ACS cells during June 2008 mixed the phytoplankton and nutrients below the euphotic depth, while providing a slower supply of nutrients into the euphotic depth in comparison to the 15 August 2003 conditions, when the MLD was shallower than the euphotic depth.

4. Discussions and Conclusions

MODIS-Aqua chlorophyll a imagery has demonstrated the development of submesoscale, high chlorophyll *a* filaments during the upwelling events of August 2003 and June 2008. These filaments are connected to the high chlorophyll water masses to the north of the Bay (Figure 1), suggesting that the advection of high phytoplankton water masses from the north might have contributed to the development of the observed submesoscale filaments. At the same time, these filaments are confined to the narrow frontal area between the cold jet and the meandering warm anticyclonic circulation offshore. This frontal area is prone to the development of the submesoscale processes and ASC cells, which are known to contribute to the development of narrow, submesoscale chlorophyll filaments in other areas of the world [see, e.g., *Calil and Richards*, 2010; *Pallàs-Sanz et al*., 2010; *Levy et al*., 2012]. As we have stated in the Introduction, it is difficult to separate the effects of advection versus in situ processes based on existing observational assets and bio-optical models, especially at submesoscale. For this reason, the focus of the paper is on whether submesoscale local processes have contributed to the intensification and dynamics of these observed filaments.

We used the vector Q_1 and the vertical velocity due to frontogenesis (W_{af}) to diagnose ageostrophic vertical motion due to frontogenesis. The leading order terms of nonlinear Ekman transport *Me* and the nonlinear Ekman pumping W_{nlep} were used to qualitatively diagnose the ageostrophic vertical motion due to nonlinear Ekman transport.

Plots of the observed and model-predicted properties across-filament (15 August 2003) have shown locations of the local maximum of Q1 (1) and the nonlinear Ekman transport *Me* (3) in the area of the observed submesoscale filament (Figure 4a). The nonlinear Ekman pumping and the vertical velocity due to frontogenesis show upwelling on the warm side of the front and downwelling on the cold jet side, which is in agreement with the development of ACS cells due to the nonlinear Ekman transport and the surface frontogenesis. The same order of W_{nlep} and W_{af} indicate that both submesoscale processes (the nonlinear Ekman pumping and the surface frontogenesis) were equally important during the formation and development of the filament. During the development of the observed chlorophyll *a* filament, both submesoscale processes had comparable time scales with the time scales of horizontal advection and with time scales of phytoplankton growth rates documented in the literature.

The observed temperature from the AUV DORADO survey has shown a flattening of isotherms as the section moves from the warm anticyclonic circulation through the frontal area. This is consistent with the surface frontogenesis, which tends to flatten the isopycnals/isotherms [see, e.g., *Klein and Lapeyre*, 2009].

Because the observed and model-predicted MLD are shallower than the estimated euphotic depth in and around the filament, the developed ASC cells kept phytoplankton in the lighted area and supported photosynthesis. Also, the ASC cells provided a vertical supply of nutrients into the euphotic area and facilitated consumption of nutrients (what was also observed by the DORADO surveys). All the above indicate that local ASC processes maintained phytoplankton population in the lighted area, supplied nutrient-rich subsurface waters into the euphotic area, and therefore facilitated the intensification and development of the

observed phytoplankton rich filament during 11–16 August 2003 (Figure 1). This provides the answer to the first question stated in the Introduction section of the paper.

Comparisons of chlorophyll *a* submesoscale filaments on 15 August 2003 and 10 June of 2008 have shown that they have similar horizontal across-filament scales. However, the maximum of the June filament chlorophyll *a* is about 3–4 times smaller than in August 2003 (Figure 1). The difference between the observed MODIS-Aqua SSTs in August and June does not alone explain the observed 3–4 magnitude difference in the intensity of phytoplankton filaments. Observations have shown that hydrographic conditions and light availability in surface and subsurface were very similar during both of the considered time periods (August 2003 and June 2008). An analysis of water samples collected along the June 2008 filament has shown that conditions were not nutrient (nitrate and silicate) limited for the phytoplankton growth. The mixed layer depth (MLD) along the June filament (∼40–60 m) was about 2–3 times deeper than the MLD during August 2003 (∼15 m), and about 10–20 m deeper than the estimated euphotic depth. Therefore, the discussed above submesoscale processes and associated ACS cells mixed the phytoplankton and nutrients below the euphotic depth in June 2008, which provided a slower supply of nutrients into the euphotic depth in comparison to the August 2003 conditions, when the MLD was shallower than the euphotic depth. During June 2008, ACS cells reduced the presence of phytoplankton in the lighted area, and therefore, reduced exposure of phytoplankton to light, and limited the growth of the filament in comparison to August 2003.

Our results show that during the late summer time frame, ASC leads to the development of phytoplankton-rich submesoscale filaments offshore, along the edge of the cold jet (when the MLD and euphotic depth are comparable)—in contrast to the earlier summer time, when the ASC mixes phytoplankton much more deeply to the depth of the MLD, which is below the euphotic depth, and submesoscale chlorophyll *a* patches are 3–4 times weaker.

Our results illustrate that during persistent upwelling favorable winds, submesoscale processes and ACS cells can modulate the development and intensification of offshore narrow (5–10 km wide) phytoplankton filaments. These submesoscale and ACS cells can incubate the phytoplankton population offshore (as for example, bioluminescent dinoflagellates during August 2003). These offshore phytoplankton filaments can migrate onshore during relaxed winds following the upwelling, and provide an additional source of phytoplankton bloom development in and around Monterey Bay. Therefore, the discussed offshore phytoplankton filaments may be a factor in the Bay ecosystem health, as for example, in the development of such events as harmful algae blooms (HABs). All these emphasize the importance of further observational and modeling studies of these submesoscale processes which impact the development and intensification of offshore submesoscale phytoplankton filaments.

Acknowledgments

This research was funded through the Naval Research Laboratory (NRL) under program element 61153N. We thank Drs. Ryan, Chavez, and Haddock of MBARI for discussions and providing observations from UUVs and moorings. We thank Brent Bartels of QinetiQ North America for help with the computer code estimating Q1 vector. We thank Dr. Barton and anonymous reviewers for providing very insightful comments and recommendations to improve the paper. Computer time for the numerical simulations was provided through a grant from the Department of Defense High Performance Computing Initiative. Request for access to the data presented in this paper can be sent to igor.shulman@nrlssc.navy.mil. This manuscript is NRL contribution 7330-14-2130.

References

Allen, J., L. Brown, R. Sanders, C. Moore, A. Mustard, S. Fielding, M. Lucas, M. Rixen, G. Savidge, and S. Henson (2005), Diatom carbon export enhanced by silicate upwelling in the northeast Atlantic, *Nature*, *437*, 728–732, doi:10.1038/nature03948.

Bellingham, J. G., K. Streitlien, J. Overland, S. Rajan, P. Stein, J. Stannard, W. Kirkwood, and D. Yoerger (2000), An Arctic basin observational capability using AUVs, *Oceanography*, *13*, 64–71, doi:10.5670/oceanog.2000.36.

Breaker, L.C., and W. W. Broenkow (1994), The circulation of Monterey Bay and related processes, *Oceanogr. Mar. Biol.*, *32*, 1–64.

Brink, K. H., R. C. Beardsley, P. P. Niiler, M. R. Abbott, A. Huyer, S. R. Ramp, T. P. Stanton, and D. Stuart (1991), Statistical properties of near surface flow in the California coastal transition zone, *J. Geophys. Res.*, *96*, 14,693–14,706.

Brzezinski, M. A. (1985), The Si:C:N ratio of marine diatoms: Interspecific variability and the effect of some environmental variables, *J. Phycol.*, *21*, 347–357.

Calil, P. H. R., and K. J. Richards (2010), Transient upwelling hot spots in the oligotrophic North Pacific, *J. Geophys. Res.*, *115*, C02003, doi:10.1029/2009JC005360.

Capet, X., J. McWilliams, M. Molemaker, and A. Shchepetkin (2008), Mesoscale to submesoscale transition in the California Current system. Part I: Flow structure, eddy flux, and observational tests, *J. Phys. Oceanogr.*, *38*, 29–43, doi:10.1175/2007JPO3671.1.

Chao, Y., et al. (2009), Development, implementation and evaluation of a data-assimilative ocean forecasting system off the central California coast, *Deep-Sea Research II*, *56*, 100–127, doi:10.1016/j.dsr2.2008.08.011.

Chavez, F. P., D. Wright, R. Herlien, M. Kelley, F. Shane, and P. G. Strutton (2000), A device for protecting moored spectroradiometers from bio-fouling, *J. Atmos. Oceanic Technol.*, *17*, 215–219.

Doyle, J. D., Q. Jiang, Y. Chao, J. Farrara (2009), High-resolution real-time modeling of the marine atmospheric boundary layer in support of the AOSNII field campaign. *Deep-Sea Research II*, *56*, 87–99, doi:10.1016/j.dsr2.2008.08.009.

Eppley, R. W. (1972), Temperature and phytoplankton growth in the sea, *Fish. Bull.*, *70*, 1063–1085.

Gould, R. W., Jr., S. C. McCarthy, I. Shulman, E. Coelho, and J. Richman (2011), Estimating uncertainties in bio-optical products derived from satellite ocean color imagery using an ensemble approach, in *Proceedings of SPIE, Remote Sensing of the Ocean, Sea Ice, Coastal Waters, and Large Water Regions 2011*, vol. 8175, edited by C. R. Bostater Jr., et al., pp. 817506-01–817506-10, doi:10.1117/12.897614.

Gruber, N., et al. (2011), Eddy-induced reduction of biological production in eastern boundary upwelling systems, *Nat. Geosci.*, *4*, 787–792, doi:10.1038/ngeo1273.
Hoskins, B. J. (1982), The mathematical theory of frontogenesis, *Annu. Rev. Fluid Mech.*, *14*, 131–151, doi:10.1146/annurev.fl.14.010182.001023.
Klein, P., and G. Lapeyre (2009), The oceanic vertical pump induced by mesoscale and submesoscale turbulence, *Annu. Rev. Mar. Sci.*, *1*, 351–375, doi:10.1146/annurev.marine.010908.163704.
Landry, M. R., M. D. Ohman, R. Goericke, M. R. Stukel, and K. Tsyrklevitch (2009). Lagrangian studies of phytoplankton growth and grazing relationships in a coastal upwelling ecosystem off Southern California, *Prog. Oceanogr.*, *83*, 208–216, doi:10.1016/j.pocean.2009.07.026.
Lapeyre, G., and P. Klein (2006), Impact of the small scale elongated filaments on the oceanic vertical pump, *J. Mar. Res.*, *64*, 835–851, doi:10.1357/002224006779698369.
Lee, Z. P., K. P. Du, and R. Arnone (2005), A model for the diffuse attenuation coefficient of downwelling irradiance, *J. Geophys. Res.*, *110*, C02016, doi:10.1029/2004JC002275.
Lee, Z. P., A. Weidemann, J. Kindle, R. Arnone, K. L. Carder, and C. Davis (2007), Euphotic zone depth: Its derivation and implication to ocean color remote sensing, *J. Geophys. Res.*, *112*, C03009, doi:10.1029/2006JC003802.
Levy, M., R. Ferrari, P. J. S. Franks, A. P. Martin, and P. Rivière (2012), Bringing physics to life at the submesoscale, *Geophys. Res. Lett.*, *39*, L14602, doi:10.1029/2012GL052756.
Mahadevan, A., and D. Archer (2000), Modelling the impact of fronts and mesoscale circulation on the nutrient supply and biogeochemistry of the upper ocean, *J. Geophys. Res.*, *105*, 1209–1225.
Martinolich, P., and T. Scardino (2011), Automated Processing System User's Guide Version 4.2, Naval Research Laboratory (NRL), Washington, D. C. [Available at http://www7333.nrlssc.navy.mil/docs/aps_v4.2/html/user/aps_chunk/index.xhtml.]
McGillicuddy, D. J., L. A. Anderson, S. C. Doney, and M. E. Maltrud (2003), Eddy-driven sources and sinks of nutrients in the upper ocean: Results from a 0.1 degree resolution model of the North Atlantic, *Global Biogeochem. Cycles*, *17*(2), 1035, doi:10.1029/2002GB001987.
Moline, M. A., S. M. Blackwell, J. F. Case, S. H. D. Haddock, C. M. Herren, C. M. Orrico, and E. Terrill (2009), Bioluminescence to reveal structure and interaction of coastal planktonic communities, *Deep Sea Res., Part II*, *56*(3–5), 232–245.
Nagai, T., A. Tandon, N. Gruber, and J. McWilliams (2008), Biological and physical impacts of ageostrophic frontal circulations driven by confluent flow and vertical mixing, *Dyn. Atmos. Oceans*, *45*, 229–251, doi:10.1016/j.dynatmoce.2007.12.001.
O'Reilly, J. E., et al. (2000), SeaWiFS Postlaunch Calibration and Validation Analyses, Part 3, in *NASA Tech. Memo. 2000–206892*, vol. 11, edited by S. B. Hooker and E. R. Firestone, 9 pp., NASA Goddard Space Flight Cent.
Paduan, J. D., and L. K. Rosenfeld (1996), Remotely sensed surface currents in Monterey Bay from shore-based HF radar (Coastal Ocean Dynamics Application Radar), *J. Geophys. Res.*, *101*, 20,669–20,686.
Paduan, J. D., K. C. Kim, M. S. Cook, and F. P. Chavez (2006), Calibration and validation of direction-finding high frequency radar ocean surface current observations, *IEEE J. Oceanic Eng.*, *862–875*, doi:10.1109/JOE.2006.886195.
Pallàs-Sanz, E., T. M. S. Johnston, and D. L. Rudnick (2010), Frontal dynamics in a California Current System shallow front: 1. Frontal processes and tracer structure, *J. Geophys. Res.*, *115*, C12067, doi:10.1029/2009JC006032.
Pennington, J. T., and F. P. Chavez (2000), Seasonal fluctuations of temperature, salinity, nitrate, chlorophyll and primary production at station H3/M1 over 1989–1996 in Monterey Bay, California, *Deep Sea Res., Part II*, *47*, 947–974.
Ramp, S. R., J. D. Paduan, I. Shulman, J. Kindle, F. L. Bahr, and F. Chavez (2005), Observations of upwelling and relaxation events in the northern Monterey Bay during August 2000, *J. Geophys. Res.*, *110*, C07013, doi:10.1029/2004JC002538.
Ramp S. R., et al. (2009), The Autonomous Ocean Sensing Network (AOSN) Predictive Skill Experiment in the Monterey Bay, *Deep Sea Res., Part II*, *56*(3–5), 8–26.
Rosenfeld, L. K., F. B. Schwing, N. Garfield, and D. E. Tracy (1994), Bifurcated flow from an upwelling center: A cold water source for Monterey Bay, *Cont. Shelf Res.*, *14*, 931–964.
Ryan, J. P., A. M. Fischer, R. M. Kudela, J. F. R. Gower, S. A. King, R. Marin III and F. P. Chavez (2009), Influences of upwelling and downwelling winds on red tide bloom dynamics in Monterey Bay, California, *Cont. Shelf Res.*, *29*, 785–795, doi:10.1016/j.csr.2008.11.006.
Shulman, I., et al. (2009), Impact of glider data assimilation on the Monterey Bay model, *Deep Sea Res., Part II*, *56*, 128–138.
Shulman, I., S. Anderson, C. Rowley, S. deRada, J. Doyle, and S. Ramp (2010), Comparisons of upwelling and relaxation events in the Monterey Bay area, *J. Geophys. Res.*, *115*, C06016, doi:10.1029/2009JC005483.
Shulman, I., M. A. Moline, B. Penta, S. Anderson, M. Oliver, and S. H. D. Haddock (2011), Observed and modeled bio-optical, bioluminescent, and physical properties during a coastal upwelling event in Monterey Bay, California, *J. Geophys. Res.*, *116*, C01018, doi:10.1029/2010JC006525.
Shulman, I., S. Frolov, S. Anderson, B. Penta, R. Gould, P. Sakalaukus, and S. Ladner (2013), Impact of bio-optical data assimilation on short-term coupled physical, bio-optical model predictions, *J. Geophys. Res. Oceans*, *118*, 2215–2230, doi:10.1002/jgrc.20177.
Thomas, L., and C. Lee (2005), Intensification of ocean fronts by downfront winds, *J. Phys. Oceanogr.*, *35*(6), 1086–1102.
Vidussi, F., H. Claustre, B. B. Manca, A. Luchetta, and J. C. Marty (2001), Phytoplankton pigment distribution in relation to upper thermocline circulation in the eastern Mediterranean Sea during winter, *J. Geophys. Res.*, *106*, 19,939–19,956.
Waterhouse, T. Y., and N. A. Welschmeyer (1995), Taxon specific analysis of microzooplankton grazing rates and phytoplankton growth rates, *Limnol. Oceanogr.*, *40*, 827–834, doi:10.4319/lo.1995.40.4.0827.